Marine Mammal Science

MARINE MAMMAL SCIENCE, **(*): ***–*** (*** 2015)

DOI: 10.1111/mms.12287

Auditory anatomy of beaked whales and other odontocetes: Potential for cochlear stimulation *via* a "vibroacoustic duct mechanism"

Duan March,[1] Faculty of Veterinary Science, The University of Sydney, Sydney, New South Wales 2006, Australia; **Daniel Brown,** Brain & Mind Research Institute, Sydney Medical School, The University of Sydney, Camperdown, New South Wales 2050, Australia; **Rachael Gray,** Faculty of Veterinary Science, The University of Sydney, Sydney, New South Wales 2006, Australia; **Ian Curthoys** and **Christopher Wong,** School of Psychology, The University of Sydney, Sydney, New South Wales 2006, Australia; **Damien P. Higgins,** Faculty of Veterinary Science, The University of Sydney, Sydney, New South Wales 2006, Australia.

Abstract

Computed tomography (CT) and microcomputed tomography (microCT) were used to examine the structures involved in cochlear stimulation in odontocetes and terrestrial mammals. Cranial CT examined the osseous attachment of the skull to the tympanoperiotic complex (TPC) and the path of the endocranial foramen of the vestibulocochlear nerve (EFVN), which was assumed to contain the perilymphatic duct. Additional CTs of TPC were taken postextraction to examine the gross morphology of this structure. MicroCT was used to examine the acoustic windows of the cochlea, including the round and oval windows and the apertures of the cochlear and vestibular aqueducts. Cranial CT scans demonstrated an osseous connection between the skull and TPC in beaked whales and *Physeter macrocephalus*. EFVN traveled through a greater length of cranial bone and communicated more closely with the periotic bone in beaked whales than in other species. *Ziphius cavirostris* was observed to have a reduced medial sulcus of the mallear ridge (MSMR) and tympanic plate and an enlarged aperture of the cochlear aqueduct, respectively. The potential significance of these findings, including the role of the perilymphatic duct as a novel route of cochlear stimulation referred to as the "vibroacoustic duct mechanism," are discussed.

Key words: beaked whale, vibroacoustic duct mechanism, perilymphatic duct, cochlear aqueduct, stranding, sonar, odontocete.

Beaked whales, in particular Cuvier's beaked whale (*Ziphius cavirostris*), have received increased scientific attention following a number of atypical stranding events associated with naval exercises using a mid-frequency active sonar (MFAS), which includes frequencies in the range of 3–8 kHz (England *et al.* 2001, Frantzis 2004, Freitas 2004, Martín *et al.* 2004, Cox *et al.* 2006, D'Amico *et al.* 2009, Filadelfo *et al.* 2009). Several hypotheses have been proposed to explain this phenomenon,

[1]Corresponding author (e-mail: duanmarch@hotmail.com).

including the unique aspects of the species' dive physiology (Zimmer and Tyack 2007), anatomical variations (Rommel *et al.* 2006), and gas emboli formation in blood vessels and internal organs (Jepson *et al.* 2003, Cox *et al.* 2006). Despite these proposed associations, a causal relationship between exposure to MFAS and atypical stranding events has not been identified.

One reason for the difficulty in defining a causal relationship between MFAS and beaked whale strandings is the uncertainty that still surrounds odontocete audition. The majority of the published data supports the "pan bone" theory of sound conduction (Norris 1968), which describes a series of specialized acoustic fats in and around the thin posterior mandible. These acoustic fats conduct vibrations to the thin ventrolateral wall of the tympanic bulla, which transfers the vibrations through the ossicular chain to the oval window of the periotic bone (Ketten 2000). Recent advances in this theory have described additional routes of sound transmission including the "gular region" in *Z. cavirostris* (Cranford *et al.* 2008), where vibrations enter the area between the left and right mandibles and travel *via* a dorsal extension of the mandibular fat body to a specialized area on the dorsolateral edge of the tympanic bulla called the medial sulcus of the mallear ridge (MSMR). This structure directly communicates with the ossicular chain and has been described as the functional analog of the terrestrial mammalian tympanic membrane (Cranford *et al.* 2010). These pathways have been demonstrated by a series of modeling studies that examined the mechanics of TPC (Hemila *et al*. 1999, Nummela *et al.* 1999) and used morphological parameters to accurately predict audiograms for a number of species (Hemilä *et al*. 2001). However, this type of analysis has not been conducted for *Z. cavirostris* or any other species of beaked whales.

An alternate mode of cochlear stimulation involving bone-conducted vibrations (BCV) has also been proposed (McCormick *et al*. 1970). This theory describes the transfer of cranial vibrations to TPC following exposure to sound, resulting in the bulk vibration of TPC and the subsequent creation of movement between the stapedial footplate and the oval window due to inertia present within the ossicular chain. This theory has been considered problematic as the cranial vibrations would equally stimulate both cochleae, resulting in no interaural intensity difference (IID) or interaural time difference (ITD), and hence, the animal would be unable to determine the direction of sound (Ketten 2000). More recently, this theory has been refined to describe the stimulation of the cochlea following bulk TPC vibration secondary to low frequency sounds delivered to TPC *via* acoustic fats (Cranford *et al.* 2010).

The stimulation of the cochlea occurs when an input creates a pressure differential between the scala media and the scala tympani. This pressure differential displaces cochlear hair cells, resulting in the stimulation of afferent neurons, which the brain interprets as sound (Echteler *et al.* 1994). A pressure difference between the scala media and the scala tympani only occurs due to the presence of the round window and/or other pressure shunts in the scala tympani; without these pressure shunts, the cochlea's sensitivity to sound is greatly diminished. In addition to the round and oval windows, the cochlea has additional communications between the cochlea and endocranial spaces, including the cochlear and vestibular aqueducts (Tonndorf 1968). A schematic representation is presented in Figure 1. These structures have been previously referred to as the "third acoustic window" of the cochlea. However, to avoid confusion with the term "acoustic window" coined by Norris (1968) and in recognition of the potential functional impact of these structures, they will hereafter be referred to as an "alternate pressure shunt mechanism."

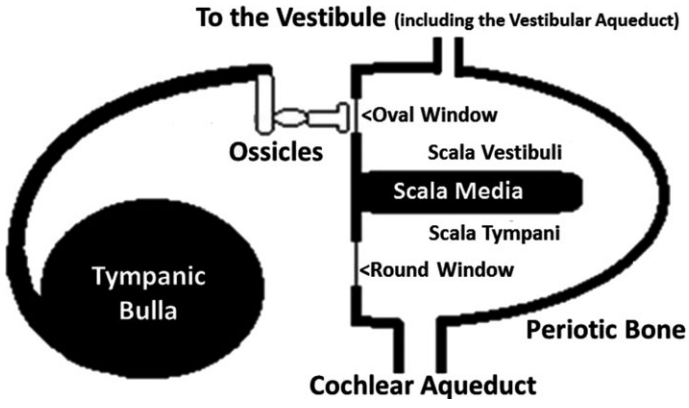

Figure 1. Schematic view of the tympanoperiotic complex and the cochlea demonstrating placement of the acoustic windows. The oval and round window account for the first two acoustic windows. The cochlear and vestibular aqueducts may also act as an "alternate pressure shunt mechanism."

In humans, the cochlear aqueduct is diminutive (Su *et al.* 1982, Gopen *et al.* 1997), and studies on the functional impact of an "alternate pressure shunt mechanism" have thus far focused on mobile windows on the scala vestibuli side of the cochlear partition, such as an enlarged vestibular aqueduct. Enlarged vestibular aqueducts result in a simultaneous decrease in sensitivity to air-conducted sounds and an increase in cochlear sensitivity to BCV (Merchant and Rosowski 2008). In addition, BCV have been shown to include a component of pressure transduction travel from the intracranial space, *via* the cochlear aqueduct, to stimulate the cochlea (Freeman *et al.* 2000, Sohmner *et al.* 2000, Sohmer and Freeman 2004). This potential route of cochlear stimulation has not been examined in odontocetes.

This study compares the auditory anatomy of *Z. cavirostris* and other odontocetes to investigate species-specific variations in cranial anatomy and TPC morphology that may have functional significance. In addition, this study examines parameters shown to be significant for BCV in terrestrial mammals and discusses the possible functional implications of these features following exposure to natural or anthropogenic sound underwater.

Materials and Methods

The specimens examined in this study were collected and archived by the Department of Primary Industry, Water and Environment (DPIWE), Tasmania, the Office of Environment and Heritage, New South Wales, and the Queensland Museum, from odontocetes that were stranded and died between 2002 and 2013.

Specimens were identified by genetic analysis conducted at the Cetacean Conservation and Genetics Laboratory, Oregon University. Species were identified from the mtDNA control region sequence using the web-based program DNA Surveillance (Ross *et al.* 2003). For those species where genetic confirmation was not available, species identification was based on morphology (Shirihai *et al.* 2006). Animals were classed as juveniles if they were equal to or shorter than the body length at weaning

as stated in the guidelines developed by the South Australian Museum (2001). The age class and species identification method for each of the species used for CT and microCT scans are listed in Table 1 and Table 2, respectively. Not all scans were performed on every animal due to the opportunistic nature of sample collection and instrument availability.

Cranial CT Scans

Archived cranial CT scans collected using established protocols (Ketten and Montie 2008) were obtained from the DPIWE for *Globicephala melas*, *Tursiops truncatus*, *Physeter macrocephalus*, *Mesoplodon layardii*, and *Mesoplodon bowdoini*. Images from cranial CT scans for *Z. cavirostris* were made available to the study courtesy of Dr. Ted Cranford, San Diego State University. The orientation of TPC relative to that of the skull is demonstrated in Figure 2. The degree of attachment between the skull and TPC and the course of the perilymphatic duct was examined. The perilymphatic duct was assumed to travel from the cranial hiatus through the EFVN to the aperture of the cochlear aqueduct on the dorsal surface of the periotic bone, as demonstrated in Figure 3. Measurements of the diameter of the perilymphatic duct were not collected at multiple points along its length due to the inadequate resolution of the CT scans for such measurements.

CT Scans of TPC

The TPC was examined using CT scans (Philips Brilliance 16-slice CT; 4535 673 86351_E, Phillips Medical Systems, Nederland BV) conducted using 120 kV and 200 mAs with a high-resolution helical scan on a thin bone setting, a section thickness of 0.8 mm, and a reconstruction advance of 0.5 mm following established guidelines (Ketten and Montie 2008). The images were stored in the Digital Imaging and Communication in Medicine format, and the three-dimensional reconstructions, volumes, and linear measurements of TPC were obtained using reconstruction software (Philips: Brilliance-Extended workspace V3.5.0.2254).

For the assessment and acquisition of TPC morphological data, CT reconstructions were rotated to provide visualization of standard landmarks as described by Kasuya (1973), including the length of the tympanic bulla (tl) as measured from the anterior spine to the posterior margin of the outer posterior prominence, the length of the periotic bone (pl) as measured from the anterior to posterior margins, and the length of the *pars cochlearis* (cl) as measured from the anterior to posterior margins of the central globular portion of the periotic bone (Fig. 4a). All linear measurements were recorded using the listed software and were performed in triplicate and then averaged. The software-generated measurements were validated against a single set of manual measurements of the tympanic, periotic, and cochlear lengths of each specimen using a Vernier caliper accurate to 0.05 mm. The volumes of the tympanic and periotic bones were also calculated using an application within the software that selected the tissue on the basis of density. Given the density of TPC, a setting of 1,000 Hounsfield units was set as the minimum density for the tissue to be included in the calculation of bone volume. The validity of the tissue selected for volume calculation was confirmed by the visual examination of concurrently displayed 2D images, which illustrated the tissue included in the calculation.

For TPCs that were articulated at the time of examination, the volume of the tympanic bulla (tv) and periotic bone (pv) were calculated by the "virtual" separation of

Table 1. Morphometric data obtained from TPC. Mean and *range* of values are listed for body length (bl), tympanic length (tl), tympanic volume (tv), periotic length (pl), periotic volume (pv), total TPC length (tpl), and the length of the *pars cochlearis* (cl). Identification (ID) of each species was established by morphological assessment (M) and where available this was used in combination with genetic sequencing (DNA). The animal age classes are juvenile (J) or nonjuvenile (NJ).

Species	ID	Age	*N*	bl (m)	tl (mm)	tv (cm^3)	pl (mm)	pv (cm^3)	tpl (mm)	cl (mm)
Globicephala melas	DNA	NJ	4 ♂	3.3	44.6	6.8	39.2	7.4	51.5	17.1
				3.1–4.6	41.9–47.3	6.2–7.8	37.1–40.9	6.6–8.0	50.0–53.9	15.9–18.5
			6 ♀	4.3	44.16	5.5	37.2	69	51.0	16.36
				3.6–4.6	43.4–45.1	4.9–6.2	36.3–37.5	6.3–7.3	49.7–51.6	16.1–16.6
		J	1 ♂	2.5	43.2	6.5	39.3	7.3	49.9	16.3
			4 ♀	2.5	41.7	5.3	37.7	7.0	49.4	16.6
				2.4–2.6	39.4–43.1	5.3–5.5	36.7–39.5	5.8–8.0	47.3–50.6	14.8–17.9
Tursiops truncatus	DNA	NJ	3 ♀	2.8	37.0	4.5	36.6	5.5	43.7	15.52
				2.6–3.0	34.5–38.3	4.4–4.5	35.8–37.7	4.9–6.7	41.3–46.1	15.2–15.7
	M	J	2 ♂	0.9	31.4	3.2	30.8	4.0	38.3	16.08
				0.9–1.0	30.2–32.5	3.2–3.2	30.6–30.9	3.9–4.0	37.7–38.8	15.9–16.2
Peponocephala electra	M	NJ	1 ♀	4.7	36.7	—[a]	33.3	—	—	14.47
Kogia sima	M	NJ	1 ♂	2.7	27.6	3.2	22.3	2.3	—	11.2
Physeter macrocephalus	DNA	NJ	1 ♂	—	58.0	3.1	59.9	31.9	—	25.6
		J	1 ♂	3.7	52.5	2.7	58.2	29.9	—	24.9
Ziphius cavirostris	M	—	3 U	—	54.05	—[a]	56.4	18.1	—	20.2
					51.5–56.3	—[a]	55.9–56.7	15.2–21.2	—	19.4–11.1
Mesoplodon hectorii	DNA	J	1 U	2.5	48.0	11.0	47.3	10.6	57.4	19.5
Mesoplodon grayii	M	NJ	1 U	5.1	42.9	—[a]	44.9	8.7	—	16.3
Mesoplodon layardii	M	NJ	1 ♂	5.9	41.6	7.5	40.3	7.0	—	15.6
		NJ	1 ♀	4.0	40.6	7.6	40.2	7.9	—	17.4
		J	1 ♀	3.6	44.2	8.0	42.3	10.9	—	20.7
Mesoplodon bowdoini	DNA	J	1 ♂	2.6	52.1	14.7	57.4	18.6	—	20.4
			1 ♀	2.4	51.1	12.3	51.1	12.2	—	20.4

[a]In some species, the posterior process of the tympanic bulla was fractured during extraction.

Table 2. Mean and *range* of values measured using cranial CT and cochlear MicroCT scans included the presence of an osseous connection between the skull and TPC (OC); the length of the perilymphatic duct (PD); and the areas of the aperture of the cochlear aqueduct (Aca), the oval window (Aow), and the round window (Arw). The ratio of each cochlear window area to the length of the periotic bone is also presented. The identification (ID) of each species was established by morphological assessment (M) and where available this was used in combination with genetic sequencing (DNA). The animal age classes are juvenile (J) or nonjuvenile (NJ).

		Cranial CT					Cochlea MicroCT							
Species	ID	Age	*N*	bl (m)	OC	(PD) (mm)	*N*	bl (m)	Aca (mm^2)	Aca:pl	Aow (mm^2)	Aow:pl	Arw (mm^2)	Arw:pl
Globicephala melas	DNA	NJ	1 ♂	3.1	N	39	—	—	—	—	—	—	—	—
			3 ♀	4.2	N	43	—	—	—	—	—	—	—	—
				3.6–4.6		34–50								
Tursiops truncatus	DNA	NJ	2 ♀	2.6–2.9	N	27–41	1 ♀	3.0	2.26	0.07	2.59	0.08	2.44	0.07
Physeter macrocephalus	M	J	1 ♂	3.7	Y	50	—	—	—	—	—	—	—	—
Kogia sima	M	NJ	1 ♂	2.7	Y[a]	—	1 ♂	2.7	0.59	0.03	1.36	0.06	1.85	0.08
Ziphius cavirostris	M	NJ	1 U	—	Y	90	1 U	—	9.07	0.16	7.08	0.13	5.72	0.10
Orcaella heinsohni	M	NJ	1 U	—	—	—	1 U	—	1.00	—	1.17	—	1.85	—
Mesoplodon bowdoini	DNA	J	1 ♀	2.5	Y	46	1 ♀	2.5	1.65	0.03	4.62	0.09	5.06	0.09
Mesoplodon layardii	M	NJ	1 ♀	4.0	Y	67	1 ♀	4.0	3.94	0.10	4.65	0.10	3.48	0.09

[a]Osseous connection was noted *via* direct observation at the time of dissection but no CT scan was performed.

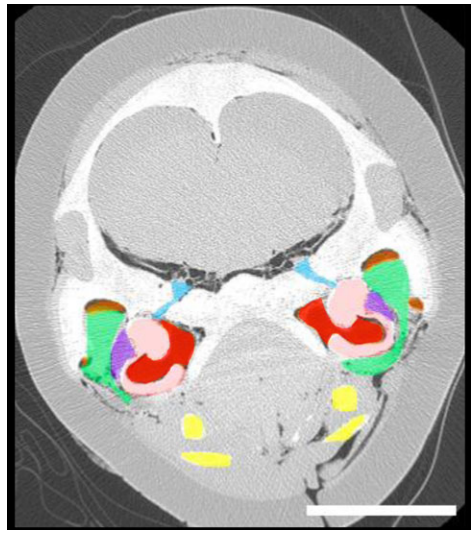

Figure 2. Transverse section of a CT scan of the head of *M. bowdoini.* The image shows the extracranial location of the tympanoperiotic complex (TPC, pink). The TPC sits within the peribullary sinus (orange), which is lined with a fibrous venous plexus (green). The hyoid apparatus is demonstrated (yellow) as is the dorsal branch of the specialized acoustic fats (purple) that communicate with the lateral plate of the tympanic bulla at the medical sulcus of the mallear ridge. The tympanic cavity (red) lies within the tympanic bulla and the epitympanic recess of the periotic bone. The endocranial foramen for vestibulocochlear nerve (blue) houses the eighth cranial nerve and potentially the perilymphatic duct and travels through the basicranium between the intracranial space and the peribullary sinus. The scale bar is 5 cm.

the bulla using the aforementioned software. The two bones were divided between the posterior processes and along the dorsolateral margin of the tympanic bulla, including the conical process, sigmoid process, and dorsal ridge of the anterodorsal crest as demonstrated in a CT reconstruction shown in Figure 4b. The quantitative measurements of MSMR were not recorded in this study due to software limitations.

MicroCT

MicroCT scans were performed on Xradia MicroXCT-400 (Xradia, Pleasanton, CA), with scanning parameters optimized on an individual basis to obtain maximum X-ray dynamic energy. Tomographical data sets were imported into hardware-based back-projection reconstruction software, supplied by Xradia, which could output serial images of 1,024 pixels in 16-bit, with a voxel resolution of 17 μm. Measurements from the microCT scans were obtained using VG-Studio Max 2 software, which allows image stacks to be rotated, thus permitting a 2D plane to be oriented for achieving ideal visualization of the parameter to be measured. Measurements collected included the area of the oval window at the footplate of the stapes, the area of the round window at the termination of the scala tympani, and the area of the aperture of the cochlear aqueduct at the point of insertion into the basal turn of the cochlea based on landmarks described in previous reports (Su *et al.* 1982, Gopen *et al.* 1997) as illustrated in Figure 5. No measurements were recorded for the aperture of

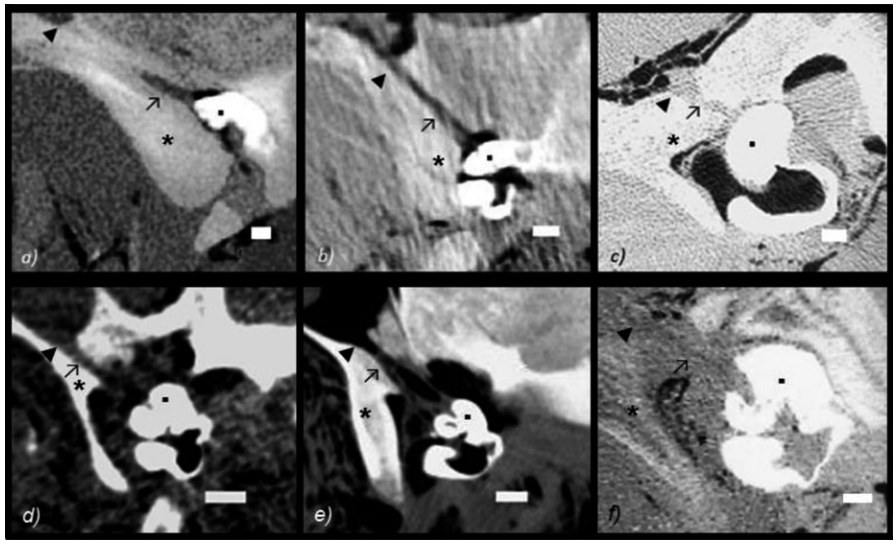

Figure 3. Magnified section of cranial CT scans showing the left endocranial foramen for vestibulocochlear nerve (↗) as it courses through the basioccipital bone (*). The membranous perilymphatic duct is assumed to run within this foramen as it courses between the aperture of the cochlear aqueduct of the periotic bone (■) and enters the intracranial space at the cranial hiatus (▶). (a) *Z. cavirostris*, (b) *M. layardii*, (c) *M. bowdoini*, (d) *T. truncatus*, (e) *G. melas*, and (f) *P. macrocephalus*. Image (a) was provided by Dr, Ted Cranford. The scale bar is 1 cm.

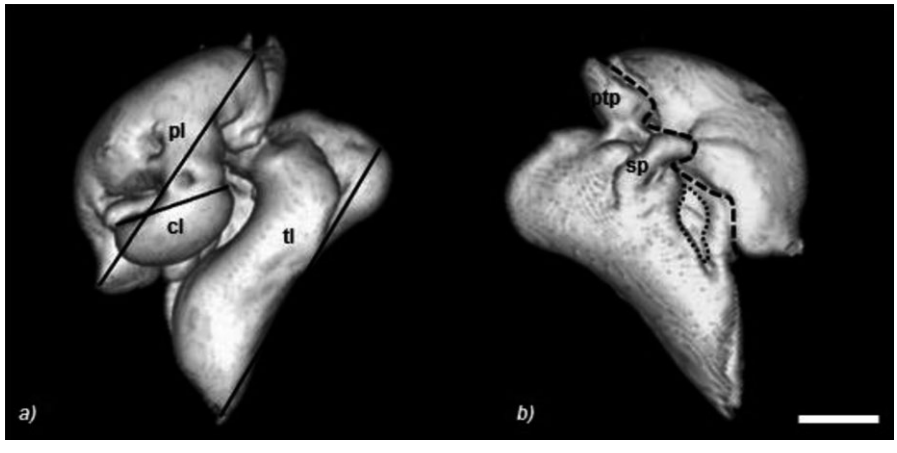

Figure 4. CT reconstructions of the *G. melas a)* medial and *b)* lateral aspects of the right tympanoperiotic complex (TPC). The image is orientated with the anterior end of the specimen facing the bottom of the image. The periotic length (pl), length of the *pars cochlearis* (cl), length of the tympanic bulla (tl), posterior tympanic process (ptp), and sigmoid process (sp) are indicated. The dashed line indicates the delineation between the tympanic bulla and the periotic bone. The dotted area shows the medial sulcus of the mallear ridge. The scale bar represents 1 cm.

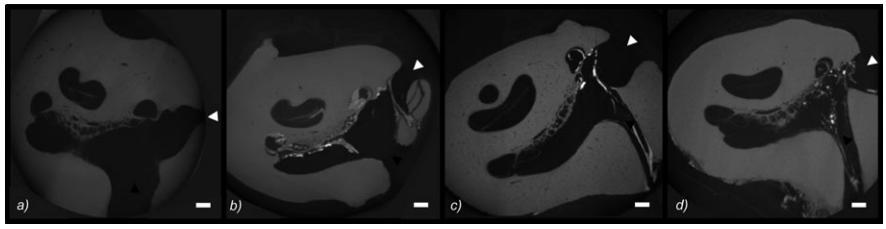

Figure 5. Microcomputed tomography scans of (a) *Z. cavirostris*, (b) *M. layardii*, (c) *M. bowdoini*, and (d) *T. truncatus*. The scans demonstrate the cochlear aqueduct (▶) at the point of entry into the basal turn of the cochlea and the round window (Δ). The scale bar is 1 mm.

the vestibular aqueduct as the structure was diminutive and poorly defined on the scans obtained.

Given that the acoustic windows were not exactly circular, the areas were calculated using the formula , where 2L represents the diameter of the short axis and 2P, the diameter of the long axis for each acoustic window (Nummela 1995). To account for allometric scaling between species, the areas of the acoustic window were also expressed as a ratio with the length of the periotic bone.

When the sample size was adequate for statistical analysis, Kruskal-Wallis *H* test (Minitab 15.1.0.0, Minitab Inc., State College, PA) was used to assess intraspecies differences and between sex and age groups. Significance was defined as $P < 0.05$.

All nomenclature is based on "The Therian Skull" (Mead and Fordyce 2009).

Results

Cranial CT Scans

The cranial CT scans showed an osseous attachment between the posterior regions of the tympanic bulla and the periotic bone of TPC and the squamosal bone of the skull in beaked whales and *P. macrocephalus* and a large amount of soft tissue surrounding TPC of *T. truncatus* and *G. melas,* as seen in Figure 3. Although the cranial CT scans were not performed for the *K. sima* specimen, a portion of the skull removed with TPC at the time of collection demonstrated a similar osseous connection. In beaked whales, the basioccipital bone was thicker and TPC was more closely aligned with its ventral surface than in the other odontocetes examined. As a result, EFVN traveled through a greater length of bone and the perilymphatic duct traveled through less soft tissue within the peribullary sinus prior to communicating with the periotic bone in beaked whales compared with the other odontocetes examined. In *P. macrocephalus,* while an osseous connection between TPC and the skull was observed, EFVN was poorly defined and appeared wider than that observed in beaked whales.

CT Scans of TPC

CT scans of TPC showed that the tympanic bulla of the four *Mesoplodon* species had a conspicuous lateral furrow, large posterior prominences with a wide interpromineal notch, and a globular outer posterior prominence. In *Z. cavirostris,* the tympanic plate lacked lateral development, was tapered and terminated caudal to the involucrum (Fig. 6). Interspecific variation in the size of MSMR relative to that of TPC was also

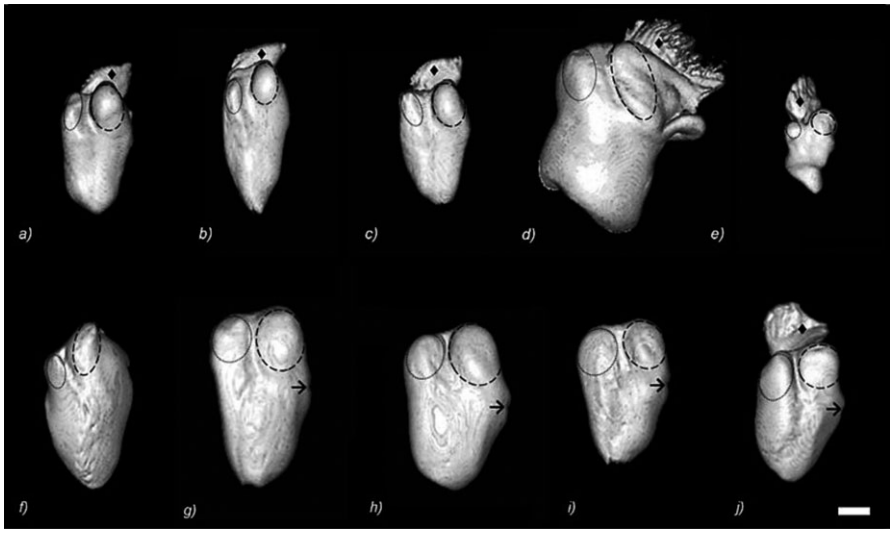

Figure 6. CT reconstructions of the ventral view of the right tympanic bulla of (a) *P. electra*, (b) *G. melas*, (c) *T. truncatus*, (d) *P. macrocephalus*, (e) *K. sima*, (f) *Z. cavirostris*, (g) *M. grayi*, (h) *M. bowdoini*, (i) *M. layardii*, and (j) *M. hectori*. Specimens are oriented with the anterior aspect toward the bottom of the image and the lateral edge to the right of each image. The inner posterior prominence is illustrated within the dotted circle and the outer posterior prominence is illustrated within the dashed circle. The lateral furrow is indicated with a black arrow, and the posterior tympanic prominence with a black diamond. The lack of posterior tympanic processes on specimens (f)–(i) are due to preparation artifacts. The scale bar is 1 cm.

observed, with this feature being smaller in *Z. cavirostris* compared with those in the other odontocetes examined (Fig. 7). MSMR of *Mesoplodon grayi* could not be assessed due to the iatrogenic separation of the tympanic bulla and the periotic bone during extraction. In *T. truncatus*, *Peponocephala electra,* and *G. melas*, the accessory ossicle was fused to the dorsomedial edge of the tympanic bulla, whereas in *P. macrocephalus, K. sima*, and the beaked whale specimens examined, the accessory ossicle was fused to the ventral surface of the periotic bone.

Interspecific variation in periotic bone morphology was also noted (Fig. 8). In beaked whales and *P. macrocephalus*, the *pars cochlearis* was delineated to a greater extent from the surrounding periotic bone, and the aperture of the cochlear aqueduct appeared large in proportion to the overall size of the periotic bone. Other odontocetes displayed *pars cochlearis* regions largely encased in the surrounding periotic bone with less obvious apertures of the cochlear aqueduct.

The sample size for *G. melas* enabled statistical investigation into biological trends. In this species, the tympanic length was found to be significantly greater in nonjuveniles ($n = 10$) compared with that in juveniles ($n = 5$) ($H = 6.08$, df = 1, $P = 0.014$). Given that there was no significant difference in the periotic length between the juvenile and nonjuvenile groups ($H = 0$, df = 1, $P = 0.947$), the two age groups were combined to investigate sex differences. The periotic length was significantly shorter in females compared with that in males ($H = 4.27$, df = 1, $P = 0.039$), despite the mean body length of the nonjuvenile females exceeding that of the male *G. melas* examined.

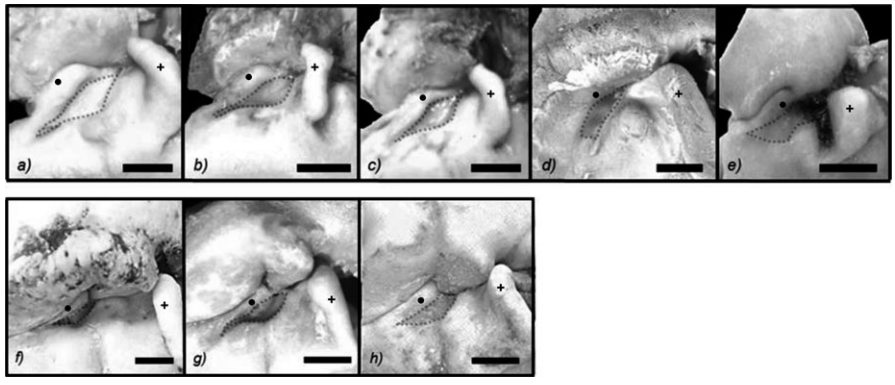

Figure 7. Lateral view of the left tympanoperiotic complex (TPC) showing the medial sulcus of the mallear ridge (MSMR). MSMR lies ventral to the anterodorsal crest (●) and cranial to the sigmoid process (+), and is outlined with a dotted line in species (a) *G. melas*, (b) *T. truncatus*, (c) *P. electra*, (d) P. *macrocephalus*, (e) *K. sima*, (f) *Z. cavirostris*, (g) *M. layardii*, and (h) *M. hectori*. The specimens are oriented with the anterior alignment facing left in each image and the periotic bone at the top of each image. The scale bar is 1 cm.

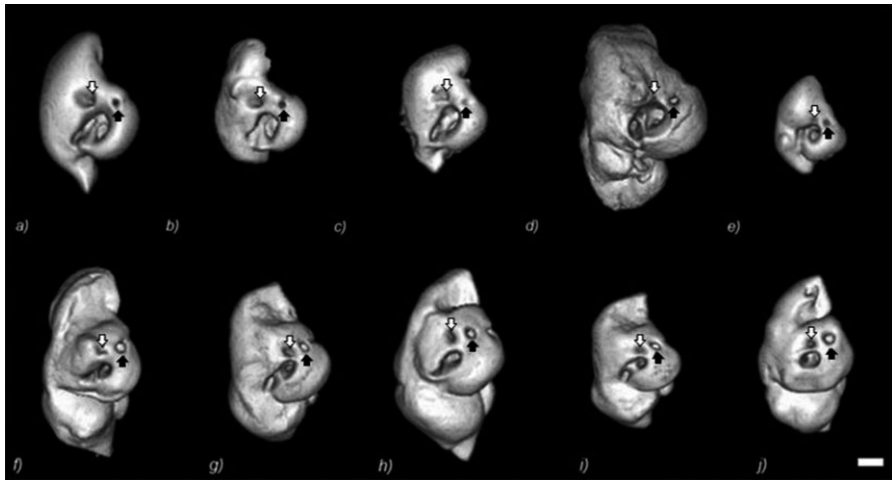

Figure 8. CT reconstructions of the dorsal view of the right periotic bone of (a) *G. melas*, (b) *T. truncatus*, (c) *P. electra*, (d) *P. macrocephalus*, (e) *K. sima*, (f) *Z. cavirostris*, (g) *M. grayi*, (h) *M. bowdoini*, (i) *M. layardii*, and (j) *M. hectori*. The specimens are oriented with the anterior process of the periotic bone towards the bottom of each image. The aperture of the cochlear aqueduct is indicated with a black arrow and the aperture of the vestibular aqueduct with a white arrow. The scale bar is 1 cm.

MicroCT

The microCT measurements of the round and oval windows and aperture of the cochlear aqueduct showed that all were larger, and larger relative to the size of the

periotic bone, in *Z. cavirostris* compared with that of the other odontocetes examined (Table 2). These results, in both absolute and relative terms, were most pronounced for the aperture of the cochlear aqueduct.

Discussion

The morphological assessment of odontocete species for which the structures of TPC have been previously described were consistent with that of previous reports (Kasuya 1973, Morell *et al.* 2007), and for the four *Mesoplodon* species that had not been previously described, the morphological features observed were consistent with descriptions of other members of this genus (Kasuya 1973). With respect to intraspecific biological trends, postnatal growth of the tympanic bulla but not the periotic bone was consistent with data reported by Kasuya (1973), but conflicted with results described by Buffrenil *et al*. (2004) and Lancaster *et al*. (2015), who stated that the full length of the tympanic bulla and periotic bone was present in newborns. The postnatal growth of the tympanic bulla predominantly occurs in the anterior spine of the bulla (Kasuya 1973) and, given that no functional significance has been attributed to this structure on the basis of anatomical modeling (Hemila 1999, Nummela 1999, Cranford *et al.* 2010), the acoustic significance of this growth postnatally is assumed to be minimal. The length of the periotic bone in female *G. melas* was shorter than that of male *G. melas*; however, the acoustic significance of this observation is presumed to be negligible.

The observation of smaller surface areas for MSMR and the tympanic plate in *Z. cavirostris* is of interest. In terrestrial mammals, the surface area of the tympanic membrane relative to that of the stapes footplate is linearly related to its sound-collecting ability, with this ratio primarily determining the middle ear transfer gain (Nummela 1995). MSMR and the tympanic plate have both been attributed to the roles of vibrational reception in odontocete similar to the tympanic membrane (Nummela 1999, Cranford *et al.* 2010). A decrease in the surface area or volume of these structures that is not matched by a relatively equal decrease in the surface area of the footplate of the stapes may decrease the sound-receiving potential and subsequent middle ear gain, thereby decreasing the efficiency of vibrational transfer through the ossicular chain. However, further investigation, including the quantitative measurements of these structures, is required before functional significance can be ascertained.

In air, mammals localize sounds on the basis of IID, ITD, and head-related transfer functions (HRTFs) with the dominant mechanism dependent on sound frequency (Blauert 1997). Underwater, these effects are markedly reduced because sound travels five times faster in water than in air and is effectively transmitted through the body/head because the tissue mechanical impedance is similar to that of water (Blauert 1997). However, despite these obstacles, odontocetes have remarkably sensitive directional hearing, being capable of detecting high-frequency sounds to within 0.9° and 0.7° in the horizontal and vertical planes, respectively (Renaud and Popper 1975).

Studies have demonstrated that the dominant mechanism of human hearing underwater is a result of BCV, where the whole skull is vibrated by sound waves (Shupak *et al.* 2005). However, tympanic transmission appears to contribute significantly to our underwater sound-localization ability (Savel *et al.* 2009). Savel *et al.* (2009) suggested that the combination of BCV and tympanic transmission results in construc-

tive/destructive interference within the cochlea. However, due to different phase combinations between the two ears, IID is effectively generated, permitting sound localization. Such a theory has only recently been considered as it pertains to how odontocetes localize sounds underwater (Schneider *et al.* 2014).

For high-frequency sounds, odontocetes are thought to utilize a complex transmission pathway and an acoustic isolation of sound through internal structures, including acoustic fats and the peribullary sinus, respectively, to generate HRTFs that enable the localization of high-frequency sounds (Norris 1968, Ketten 1997, Mooney *et al.* 2012). However, for low-frequency (<100 Hz) sounds, these complex HRTF mechanisms are most likely negligible (Mooney *et al.* 2012). Given that both BCV and vibrations transmitted through acoustic fats simultaneously contribute to cochlear stimulation, it is plausible that interactions between the different transmission modes may interfere at the level of the cochleae. This interference may result in constructive/destructive combinations in either cochlea and may potentially create an apparent IID in odontocetes, as has been suggested to occur in humans underwater (Savel *et al.* 2009).

The observed hypertrophy of the aperture of the cochlear aqueduct in *Z. cavirostris* may reflect an enlarged membranous perilymphatic duct and is of potential significance to cochlear stimulation and sound localization. In terrestrial mammals, the cochlear aqueduct communicates between the intracranial space and the cochlea *via* the fluid-filled perilymphatic duct and is capable of transmitting acoustic energy to the cochlea (Freeman *et al.* 2000, Sohmner *et al.* 2000, Sohmner and Freeman 2004) and has lower impedance at low frequencies (Gopen *et al.* 1997) and may represent a novel route of sound conduction in odontocetes. Cranford *et al.* (2010) proposed a low-frequency model of cochlea stimulation created by the bulk motion of TPC and the subsequent inertial lag of the stapes. However, the first frequencies that created these natural modes of vibration were recorded at the relatively high frequencies of 8.1 kHz and 10 kHz for *T. truncatus* and *Z. cavirostris*, respectively. Hence, the stimulation of the cochlea at frequencies lower than these modes must be occurring *via* a different route, potentially *via* the transmission of acoustic energy to the cochlea *via* the intracranial space *via* the perilymphatic duct; we have termed this the "vibroacoustic duct mechanism."

If the enlarged aperture of the cochlear aqueduct observed in *Z. cavirostris* is reflective of an enlarged perilymphatic duct entering the scala tympani, the functional significance of this structure acting as an "alternate pressure shunt mechanism" is of interest. The impedance of the scala tympani is lower than that of the scala vestibuli (Merchant *et al.* 1996), and the addition of a patent aperture of the perilymphatic duct would further increase this difference, which may increase the sensitivity of acoustic energy transmitted to the cochlea *via* the ossicular chain. Given the uncertainty surrounding the ability of odontocetes to maintain a uniform middle ear impedance during deep dives, the impact of this "alternate pressure shunt mechanism" may vary during the dive profile.

Further research is required to better describe the anatomy of the vestibular and perilymphatic ducts in odontocetes before the functional significance of these structures can be evaluated. This needs to include the calculation of the impedance of the perilymphatic duct to assess of the potential impact that this structure will have as as an "alternate pressure shunt mechanism" for vibrational energy delivered *via* the ossicular chain as well as the potential for this structure to stimulate the cochlea *via* the "vibroacoustic duct mechanism." This will enable modeling for each species at

various frequencies, including those used during MFAS, and may reveal a novel route of cochlear stimulation in odontocetes.

Acknowledgments

Special thanks to Dr. Rosemary Gales, Dr. Isabel Beasley, Drew Lee, and Andrew Irvine for the collection of many of the samples used in this project. Special thanks also to Adjunct Assistant Professor Ted Cranford, San Diego State University, who provided the computed tomography scan of the head of *Z. cavirostris*. We also thank The Australian Centre for Microscopy and Microanalysis at The University of Sydney for access to and assistance in using their imaging facilities, and in particular, Dennis Dwarte and Dr. Matthew Foley. We also thank Helen Laurendet of the Faculty of Veterinary Science at The University of Sydney for providing her time and expertise in the production of the CT scans. We also thank Dolphin Marine Magic for the provision of in-kind support during the study. We thank the anonymous reviewers for their comments on the manuscript.

Literature Cited

Blauert, J. 1997. Spatial hearing: The psychophysics of human sound localization. MIT Press, Cambridge, MA.

Buffrenil, V., W. Dabin and L. Zylberberg. 2004. Histology and growth of the cetacean petro-tympanic bone complex. Journal of Zoology 262:371–381.

Cox, T. M., T. J. Ragen, A. J. Read, *et al*. 2006. Understanding the impacts of anthropogenic sound on beaked whales. Journal of Cetacean Resource Management 7:177–187.

Cranford, T. W., M. F. Mckenna, M. S. Soldevilla, *et al*. 2008. Anatomic geometry of sound transmission and reception in Cuvier's beaked whale (*Ziphius cavirostris*). The Anatomical Record: Advances in Integrative Anatomy and Evolutionary Biology 291:353–378.

Cranford, T. W., P. Krysl and M. Amundin. 2010. A new acoustic portal into the odontocete ear and vibrational analysis of the tympanoperiotic complex. PLOS ONE 5:e11927.

D'Amico, A., R. C. Gisiner, D. R. Ketten, J. A. Hammock, C. Johnson, P. L. Tyack and J. Mead. 2009. Beaked whale strandings and naval exercises. Aquatic Mammals 35:452–472.

Echteler, S. M., R. R. Fay and A. N. Popper. 1994. Structure of the mammalian cochlea. Pages 134–171 *in* R. R. Fay, ed. Comparative hearing: Mammals. Springer, New York, NY.

England, G., D. Evans, C. Lautenbacher, S. Morriessy and W. Hogarth. 2001. Joint interim report Bahamas marine mammal stranding event of 15–16 March 2000. U.S. Department of Commerce, U.S. Secretary of the Navy.

Filadelfo, R., J. Mintz, E. Michlovich, A. D'Amico, P. L. Tyack and D. R. Ketten. 2009. Correlating military sonar use with beaked whale mass strandings: What do the historical data show? Aquatic Mammals 35:435–444.

Frantzis, A. 2004. The first mass stranding that was associated with the use of active sonar, Kyparissiakos Gulf, Greece, 1996. European Cetacean Society Newsletter 42:14–20.

Freeman, S., J. Y. Sichel and H. Sohmer. 2000. Bone conduction experiments in animals–evidence for a non-osseous mechanism. Hearing Research 146:72–80.

Freitas, L. 2004. The stranding of three Cuvier's beaked whale (*Ziphius cavirostris*) in Madeira Archipelago—May 2000. European Cetacean Society Newsletter 42:28–32.

Gopen, Q., J. J. Rosowski and S. N. Merchant. 1997. Anatomy of the normal human cochlear aqueduct with functional implications. Hearing Research 107:9–22.

Hemilä, S., S. Nummela and T. Reuter. 1999. A model of the odontocete middle ear. Hearing Research 133:82–97.

Hemila, S., S. Nummela and T. Reuter. 2001. Modelling whale audiograms: Effects of bone mass on high-frequency hearing. Hearing Research 151:221–226.

Jepson, P., M. Arbelo, R. Deaville, *et al*. 2003. Gas-bubble lesions in stranded cetaceans. Nature 425:575–576.

Kasuya, T. 1973. Systematic consideration of recent toothed whales based on the morphology of tympano-periotic bone. Scientific Reports of the Whales Research Institute, Tokyo 25:1–103.

Ketten, D. R. 1997. Structure and function of whale ears. Bioacoustics 8:103–135.

Ketten, D. R. 2000. Cetacean ears. Pages 43–108 *in* W. Au, A. Popper and R. Fay eds. Hearing by whales and dolphins. Springer, New York, NY.

Ketten, D., and E. Montie. 2008. Imaging procedures for stranded marine mammals. Woods Hole Oceanograhic Institute: Technical Report WHOI-2008-02.

Lancaster, W. C., W. J. Ary, P. Krysl and T. W. Cranford. 2015. Precocial development within the tympanoperiotic complex in cetaceans. Marine Mammal Science 31:369–375.

Martín, V., A. Servidio and S. García. 2004. Mass strandings of beaked whales in the Canary Islands. European Cetacean Society Newsletter 42:33–36.

McCormick, J. G., E. G. Wever, J. Palin and S. H. Ridgway. 1970. Sound conduction in the dolphin ear. The Journal of the Acoustical Society of America 48:1418–1428.

Mead, J. G., and R. E. Fordyce. 2009. The therian skull: A lexicon with emphasis on the odontocetes. Smithsonian Contributions to Zoology 627:1–248.

Merchant, S. N., and J. J. Rosowski. 2008. Conductive hearing loss caused by third-window lesions of the inner ear. Otology and Neurotology 29:282–289.

Merchant, S. N., M. E. Ravicz and J. J. Rosowski. 1996. Acoustic input impedance of the stapes and cochlea in human temporal bones. Hearing Research 97:30–45.

Mooney, T. A., M. Yamato and B. K. Branstetter. 2012. Hearing in cetaceans: From natural history to experimental biology. Advances in Marine Biology 63:197–246.

Morell, M., E. Degollada, M. Van Der Schaar, *et al*. 2007. Comparative morphometry of odontocete ears through computerized tomography. Journal of the Marine Biological Association of the United Kingdom 87:69–76.

Norris, K. 1968. The evolution of acoustic mechanisms in odontocete cetaceans. Pages 297–324 *in* E. T. Drake, ed. Evolution and environment. Yale University Press, New Haven, CT.

Nummela, S. 1995. Scaling of the mammalian middle ear. Journal of Speech, Language and Hearing Research 85:18–30.

Nummela, S., T. Wagar, S. Hemila and T. Reuter. 1999. Scaling of the odontocete middle ear. Journal of Speech, Language and Hearing Research 133:71–81.

Renaud, D. L., and A. N. Popper. 1975. Sound localization by the bottlenose porpoise *Tursiops truncatus*. The Journal of Experimental Biology 63:569–585.

Rommel, S. A., A. M. Costidis, A. Fernandez, *et al*. 2006. Elements of Beaked whale anatomy and diving physiology and some hypothetical causes of sonar-related stranding. Journal of Cetacean Research and Management 7:189–209.

Ross, H. A., G. M. Lento, M. L. Dalebout, *et al*. 2003. DNA surveillance: Web-based molecular identification of whales, dolphins, and porpoises. Journal of Heredity 94:111–114.

Savel, S., C. Drake and G. Rabau. 2009. Human auditory localization in a distorted environment: Water. Acta Acoustica United with Acoustica 95:128–141.

Schneider, J. N., D. R. Lloyd, P. N. Banks and E. Mercado. 2014. Modeling the utility of binaural cues for underwater sound localization. Hearing Research 312:103–113.

Shirihai, H., B. Jarrett and G. M. Kirwan. 2006. Whales, dolphins, and other marine mammals of the world. Princeton University Press, Princeton, NJ.

Shupak, A., Z. Sharoni, Y. Yanir, Y. Keynan, Y. Alfie and P. Halpern. 2005. Underwater hearing and sound localization with and without and air interface. Otology and Neurotology 26:127–130.

Sohmer, H., and S. Freeman. 2004. Further evidence for a fluid pathway during bone conduction auditory stimulation. Hearing Research 193:105–110.
Sohmer, H., S. Freeman, M. Geal-Dor, C. Adelman and I. Savion. 2000. Bone conduction experiments in humans–a fluid pathway from bone to ear. Hearing Research 146:81–88.
South Australian Museum. 2001. Guide to dependant young: Weaning lengths, South Australian cetacean species. Appendix 3 *in* D. P. Higgins and M. J. Noad, eds. Standardised protocols for the collection of biological samples from stranded cetaceans. Australian Government Department, Environment and Heritage, Canberra, Australia.
Su, W. Y., M. S. Marion, R. Hinojosa and G. J. Matz. 1982. Anatomical measurements of the cochlear aqueduct, round window membrane, round window niche and facial recess. The Laryngoscope 12:483–486.
Tonndorf, J. 1968. A new concept of bone conduction. Acta Oto-Laryngologica 87:49–54.
Zimmer, W. M., and P. L. Tyack. 2007. Repetitive shallow dives pose decompression risk in deep-diving Beaked whales. Marine Mammal Science 23:888–925.

Received: 14 May 2015
Accepted: 30 September 2015